Jet-cooled infrared spectrum of methoxy in the CH stretching region†‡§

Jiaxiang Han,[a] Shuiming Hu,[b] Hongbing Chen,[a] Yurii Utkin,[a] John M. Brown[c] and Robert F. Curl*[a]

Received 12th January 2007, Accepted 9th March 2007
First published as an Advance Article on the web 3rd April 2007
DOI: 10.1039/b700502d

Observations of the jet-cooled infrared spectrum of CH_3O in the CH stretching region have been extended, down to 2756 cm^{-1} and up to 3003 cm^{-1}. In the lower frequency extension, a single vibronic band has been assigned. In the higher frequency region, the spectrum becomes complex above 2900 cm^{-1} and remains so until near 2970 cm^{-1} where it rapidly becomes sparse. Including the single vibronic band previously reported, a total of four bands have been assigned. Two bands including the original one follow a perpendicular $\Delta P = +1$ rotational selection rule and the other two bands follow a parallel $\Delta P = 0$ selection rule. In addition to these in the congested region between 2900 and 2970 cm^{-1}, ten isolated sub-bands (two $P'' = -1/2$, two $P'' = +1/2$, and six $P'' = +1.5$) have been assigned, but it has so far not been possible to connect these together to form bands. Taken together these observations suggest that there are strong vibronic couplings between the two CH stretching vibrations and the overtone and combination levels in the region.

A. Introduction

Methoxy radical (CH_3O) is *the* classic example of Jahn–Teller coupling. Consequently numerous works concerned with the spectroscopy of this molecule have been published. The review article on Jahn–Teller coupling by Barckholtz and Miller[1] provides references of the spectroscopic work on this molecule up until 1998. In spite of this intense effort, no rotational analysis of a complete perpendicular vibrational band of this molecule has appeared. The work described here (and its previously reported first instalment[2]) was initiated in order to fill this gap by obtaining and analyzing the CH stretching fundamental ν_4. We are chagrined to report that this goal remains as distant as ever. We have started too high in the energy manifold; the ν_4 spectrum in the CH stretching region is heavily affected by interactions with overtone and combination bands and probably by interaction with the symmetric CH stretching fundamental ν_1.

From the point of view of avoiding such interactions, it would have been better to start with ν_6. However, the technical challenge of obtaining monochromatic tunable infrared laser radiation over the entire region of ν_6 is formidable. Perhaps this spectrum might be obtained using time-resolved Fourier-transform spectroscopy. If so, even the room temperature spectrum should be analyzable through reliance on the well-known ground state combination differences.

In spite of our disappointment over not being able to report a complete analyzed spectrum for ν_4, the observations reported here tell us something about CH_3O and provide several puzzles that may engage other spectroscopists.

B. Experimental

The experimental apparatus and methods have been described previously[2,3], and will only be sketched here. Fig. 1 shows the apparatus. The two UV mirrors and a long focal length BaF_2 lens used to direct the excimer to the slit have been omitted from Fig. 1. Methyl nitrite was seeded (~2%) into first run neon (~70% Ne and ~30% He) at a backing pressure of ~0.7 bar. Upon firing of the valve (General Valve Corp. series 9) a gas pulse of ~1 ms duration was produced with a repetition rate of ~10 Hz. The excimer laser pulse (~100 mJ, 248 nm, KrF) was fired in the middle of the gas pulse photolyzing the CH_3ONO in the gas emerging from a 2 cm slit creating CH_3O

$$CH_3ONO + h\nu \rightarrow CH_3O + NO \qquad (1)$$

Supersonic expansion cooled the emerging CH_3O to approximately 26 K in the region where the infrared probe traverses the expanding jet approximately 1.4 cm downstream from the nozzle orifice.

The infrared probe radiation (~40 μW) was produced by mixing the fundamental of a single mode Nd:YAG (1064 nm) with the output of a scanning Ti:sapphire laser (Coherent Autoscan™ Model 899-29) in a 19 mm long crystal of periodically poled $LiNbO_3$ (PPLN). The step size of the scans was 10 MHz. After a fraction of the emerging infrared was split off as a reference, the remaining probe beam traversed a short Herriot cell surrounding the supersonic jet 27 times giving an effective pathlength of 54 cm before it impinged on a liquid

[a] *Chemistry Department and Rice Quantum Institute, Rice University, Houston, TX 77005, USA. E-mail: rfcurl@rice.edu; Fax: 1 713 348 5155; Tel: 1 713 348 4816*
[b] *Hefei National Laboratory for Physical Sciences at the Microscale, Department of Chemical Physics, University of Science and Technology of China, Hefei, China. E-mail: smhu@ustc.edu.cn; Fax: (86)551-3602969*
[c] *Department of Physical Chemistry, Oxford University, Oxford, UK. E-mail: jmb@physchem.ox.ac.uk; Fax: 44 1865 275410*
† This work supported by grants from the Robert A. Welch Foundation and National Science Foundation Grant CHE-0111125.
‡ The HTML version of this article has been additionally enhanced with colour images.
§ Electronic supplementary information (ESI) available: A complete listing of all assigned lines in text format. See DOI: 10.1039/b700502d

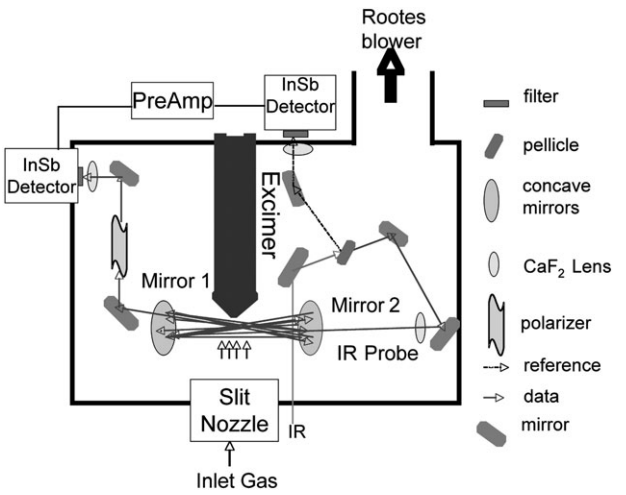

Fig. 1 Jet cooled radical IR absorption apparatus.

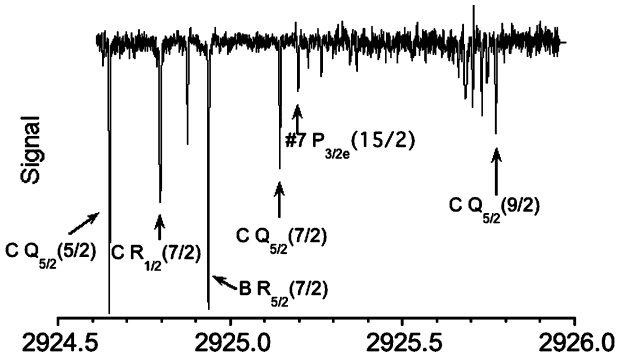

Fig. 2 Example scan. Labels are explained in text.

nitrogen cooled InSb detector. A second such detector of opposite polarity was attached to the input of the transimpedance preamplifier to null out both the DC offset and the noise arising from amplitude fluctuations of the probe. The polarizer depicted in Fig. 1 was used to null the DC signals from the two detectors. After passing through a high pass filter, the preamplifier output was acquired by a transient digitizer triggered by the firing of the excimer. After each pulse, the transient digitizer datum was stored.

The frequency scale was calibrated by simultaneously acquiring the infrared absorption spectrum of a reference gas and the fringe spacings of a 0.025354 cm^{-1} FSR etalon placed in a portion of the Ti:sapphire output. For the longer wavelengths, jet H_2CO produced in the photolysis together with CH_4 in a separate cell were the reference gases; for the shorter wavelengths C_2H_4 was the reference gas. The frequencies of the absorption lines of the reference gases were obtained from the HITRAN tabulation.[4]

C. Observations

The peaks of transient absorptions of the gases emerging from the jet were delayed by about 15 μs from the excimer flash because of the time required for the species to traverse the distance from nozzle face to probe region. Generally these absorption signals showed two kinds of behavior. CH_3O absorptions decayed rapidly after peaking presumably because CH_3O produced inside the nozzle reacted extensively under the high radical concentrations inside the nozzle. Other lines were observed having absorptions that lingered for tens of μs after peaking. Most of these were identified as belonging to ground state H_2CO and a few to ground state CH_3OH.

When frequency scans were examined, three time channels were employed. A 5 μs time window at 15 μs after the flash contained signals from both the transient molecules (CH_3O and vibrationally excited H_2CO) as well as signals from ground state H_2CO. By the time of a later 5 μs time window at 20 μs after the flash, the CH_3O signals had decayed significantly. This permitted the separation of signals from transient species from those of non-reactive species. The signal-to-noise of lines in both of these channels was improved by subtracting a 5 μs time window at 12 μs after the flash, a point well before the peak of the CH_3O absorption thus removing low frequency noise associated with laser intensity fluctuations.

Fig. 2 shows an example scan. Almost all lines in this scan have the transient species time dependence. The lines marked 'B' and 'C' belong to band systems described below. The line marked #7 belongs to an isolated sub-band given in the supplementary material. The unmarked lines have not been assigned.

Many of the lines belonging to transients in the low frequency region 2760 to 2830 cm^{-1} could be identified as belonging to vibrationally excited H_2CO.[5] Aside from H_2CO and CH_3O, no other bearer of transient lines could be identified. This does not rule out lines from other transient molecules, as many transient lines remain unassigned. Fig. 3 is a histogram illustrating the density of transient lines; assigned lines of vibrationally excited H_2CO have been removed. There are quite a few transient lines below 2840 cm^{-1}, but it is only above this frequency that lines appear of the lowest frequency sub-band that can be clearly identified through ground state

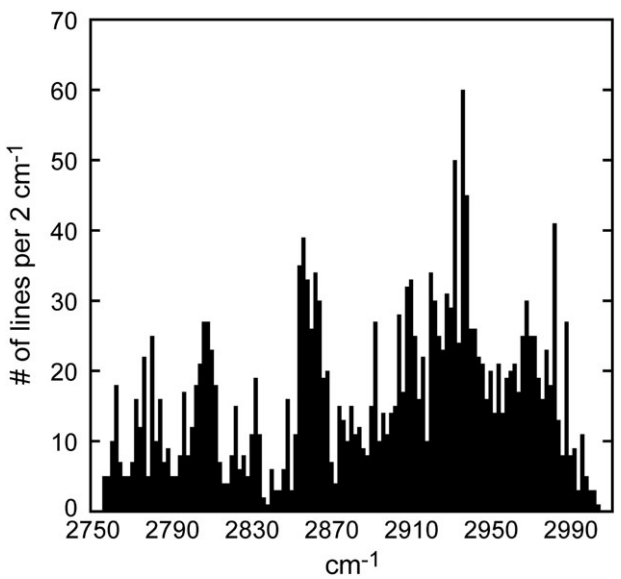

Fig. 3 Histogram of transient absorption lines.

combination differences as arising from CH_3O. The density of CH_3O lines gradually increases with increasing frequency peaking near 2935 cm^{-1}. Above 2970 cm^{-1}, the line density rapidly decreases until no transient lines appear above 3003 cm^{-1}. Scanning was stopped at 3010 cm^{-1}.

D. Expectations

The ground state is split into two components separated by 62 cm^{-1} (cm^{-1} will be the energy units used throughout) by the spin–orbit interaction. The probe region temperature is sufficiently low ($\sim$26 K) that transitions from the upper spin–orbit $^2E_{1/2}$ component of the ground vibronic state are expected to be too weak to be observable. The symmetric CH stretching mode (ν_1) is expected to be split into two levels by the spin–orbit effect by analogy to the ground vibronic state with the lower level of vibronic symmetry $E_{3/2}$ and the upper $E_{1/2}$. The splitting is expected to be similar to the ground state. As discussed in our first paper on this subject,[2] the E symmetry unsymmetrical CH stretching mode (ν_4) of CH_3O is expected to split into four vibronic modes through the combination of spin–orbit and Jahn–Teller splittings.

The vibronic structure of the ground state of CH_3O has been the subject of six recent theoretical papers.[6–11] The recent extensive paper[10] by Marenich and Boggs provides detailed quantitative predictions of the CH stretching level structure. These are shown in Fig. 4. The predicted harmonic energies for the symmetric CH stretch ω_1 and the unsymmetrical stretch ω_4, are leftmost. The introduction of anharmonicity shifts these levels downward by about 100 cm^{-1}. The Jahn–Teller interactions in methoxy arise because the orbital angular momentum about the threefold symmetry axis is not completely quenched. In setting up the quantum mechanical problem of the rovibronic levels of CH_3O, the quantum number Λ with possible values of ±1 is included in the basis to account for this. Methoxy also has an unpaired electron. Because the electron spin–orbit interaction is usually stronger than end-over-end spin-rotation Coriolis interaction (nearly Hund's case (a)), the quantum number Σ with values $\pm1/2$ representing the projection of the electron spin on the symmetry axis is introduced into the basis. In addition, when a degenerate vibration such as ν_4 is excited, the vibrational angular momentum about the threefold axis may be non-zero. Therefore the quantum number l with integer values with (for our case) $l_4 = \pm1$ is introduced. Positive l corresponds to rotation in the same direction as positive Λ. For the vibronic problem, these suffice to define a basis. Thus in the middle level scheme in Fig. 4, where the effects of the first order Jahn–Teller interaction and the spin–orbit interaction are introduced, the $v_4 = 1$ levels are labeled by $|\Lambda + l|$. There are two levels for each value of $|\Lambda + l|$ corresponding to the two possible values of Σ with $\Sigma = +1/2$ the lower.

In the rightmost set of levels in Fig. 4, two additional interactions have been introduced: second order Jahn–Teller (blue double arrow) and the bilinear Jahn–Teller interaction between ν_4 and ν_1 (red double arrow). (Note: the longest double red arrow connects to highest level.) The rightmost levels are exactly the final predictions of Marenich and Boggs.[10] Assuming, as Marenich and Boggs found, that the

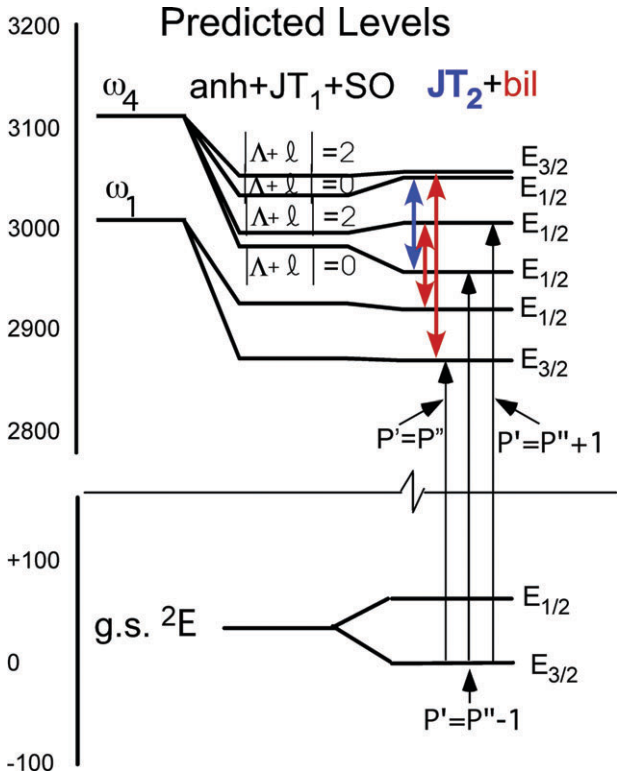

Fig. 4 Expected CH stretch levels and transitions based on ref. 10.

mixings due to second order Jahn–Teller and bilinear Jahn–Teller are fairly small, only the three transitions from the ground state shown are expected to have appreciable intensity because Σ is a good quantum number in the absence of rotation.

For our rotationally resolved spectra, we must introduce two additional rotational quantum numbers, J (the total angular momentum) and P (the total angular momentum about the threefold axis). A rotational assignment of a line consists of labeling it with (J', P') and (J'', P''), which are the rotational quantum numbers of the upper and lower states, respectively.

As noted in Fig. 4, the selection rules for the rotational quantum number P are determined by which vibronic transition (black arrows in Fig. 4) is observed. The symmetric vibration ν_1 should have its electric dipole transition moment directed along the symmetry axis resulting in parallel selection rules where $P' = P''$. The electric dipole transition moment for the unsymmetrical vibration ν_4 is expected to be perpendicular to the symmetry axis giving rise to perpendicular selection rules like $P' = P'' \pm 1$. However, unlike an ordinary symmetric top, changing the sign of P changes the energy significantly. The selection rules in P are also signed as shown in Fig. 4 where the center arrow has $P' = P'' - 1$ and the right arrow has $P' = P'' + 1$.

The mixing represented by the blue and red arrows can lend some of the intensity of the allowed transitions to the other level in the mixing. It turns out that mixing for both cases is between J, P and J, $-P$. Thus transitions to the uppermost level allowed by mixing with longest red arrow will have

selection rule $P' = -P''$, a form of parallel selection rules, while transitions to the next to lowest level allowed by the mixing associated with the other red arrow have selection rules $P' = -P'' - 1$. Transitions to the next to highest level allowed by the blue arrow will have selection rules $P' = -P'' + 1$.

Once a band is assigned, which rotational selection rules apply can be determined from presence or absence of lines and/or relative intensities. In discussing assignments, we will sometimes refer to the C_{3v} symmetry label of a rovibronic level, A_1, A_2, or E. A_1 and A_2 levels are expected to always come in pairs. A_1, A_2 pairs occur for $P - \Lambda - \Sigma - l = 0$ modulo 3; E levels for $P - \Lambda - \Sigma - l = \pm 1$ modulo 3. If for one J value the A_1 level of the pair is above the A_2 level, for the next J value this ordering is reversed. For the convenience of the spectroscopist, the concept of "rotationless symmetry" and the labeling of levels by e or f is introduced. If the level is of symmetry A_1 and $J - 1/2$ is even, the level is labeled e; if for an A_1 level, $J - 1/2$ is odd, the level is labeled f. For A_2 levels, this labeling scheme is reversed so that the levels are expected to appear in e, f pairs without the irritating oscillation in labeling upon moving from one J value to the next.

E. Assignments

Each sub-band was assigned by use of ground state combination differences. These are particularly useful because the effective B values depend enough on the P quantum number to determine P'' entirely from the $E_{3/2}$ ground state combination differences. These combination differences were calculated using the constants of Liu *et al.*[12] and are tabulated in Table 1. The output of the program calculating the ground state energies were checked against the hyperfine structure averaged microwave transition frequencies of Endo, Saito, and Hirota.[13]

When ground state combination differences can be measured for the three lines $R_P''(J' - 1) - P_P''(J' + 1)$, $R_P''(J' - 1) - Q_P''(J')$, $Q_P''(J') - P_P''(J' + 1)$, the P'' value of the sub-band can be uniquely identified from ground state combination difference values alone and the upper state energy levels can be calculated by adding the appropriate ground state energy and averaging the result from the two or three transitions accessing the same upper state level. To fix the upper state energies, we set the energy of the lowest ground state level, $P = +1/2$, $J = 1/2$ to zero.

A quadratic in $J'(J' + 1)$ is then fitted to the energies of the sub-band thus determined giving the hypothetical $J' = 0$ energy, E_0, of the sub-band and effective B' and D' values.

In order to assign a band, several sub-bands corresponding to different values of P' have to be found to be related. If at least three sub-bands were felt to be related, a quadratic in P' was fitted to the values of $E_0(P')$ to guide the process of linking in other sub-bands. Nominally the curvature of such a quadratic should equal $(A - B)$, which for the ground state is 4.24 cm^{-1}. However, curvature can be affected by parallel Coriolis interactions. For example, for levels stemming from ν_4 $|\Lambda + l| = 0$, under the influence of a large second order Jahn–Teller, the normal Coriolis interaction of the ground state shifts to off-diagonal and its second order result is to flatten the lower level curvature and increase the upper level curvature. However, we were never able to assign either of these two bands.

In the less congested regions below 2900 cm^{-1} and above 2970 cm^{-1}, the likelihood of assuming a false relationship between sub-bands is small, but in the congested region the probability is much higher of creating an erroneous band from a collection of sub-bands that are individually correctly assigned.

Band assignments

We have been able to collect together only 18 of the P sub-bands to form four bands including the one previously reported.[2] This older band is centered near 2890 cm^{-1} and has $P + 1 \leftarrow P$ selection rules. We now call this original band, 'B'. One band system, 'A', which is somewhat weaker than the one previously reported, is found below it centered near 2860 cm^{-1} and again has $P + 1 \leftarrow P$ selection rules. The other two bands, 'C' and 'D', have parallel ($P \leftarrow P$) selection rules, are rather

Table 1 Ground state CH_3O combination differences (cm^{-1})

P''	−1.5[a]	−0.5	+0.5	+1.5 u.s. f[b]	+1.5 u.s. e[b]	+2.5
PR diffs						
$J' = 1.5$		7.3290	7.3357			
2.5	10.9769	10.9937	11.0036	11.0135	11.0058	
3.5	14.6367	14.6587	14.6716	14.6863	14.6728	14.6840
4.5	18.2973	18.3240	18.3398	18.3600	18.3390	18.3549
5.5	21.9585	21.9896	22.0081	22.0345	22.0044	22.0258
6.5	25.6208	25.6557	25.6766	25.7097	25.6691	25.6965
7.5	29.2837	29.3222	29.3451	29.3856	29.3331	29.3672
PQ diffs						
$J' = 0.5$		2.7483	2.7509			
1.5	4.5736	4.5806	4.5848	4.5895	4.5852	
2.5	6.4033	6.4131	6.4188	6.4283	6.4163	6.4243
3.5	8.2334	8.2456	8.2528	8.2700	8.2445	8.2597
4.5	10.0639	10.0783	10.0870	10.1155	10.0690	10.0952
5.5	11.8946	11.9113	11.9212	11.9655	11.8889	11.9306
6.5	13.7261	13.7444	13.7554	13.8208	13.7036	13.7659

[a] A_1, A_2 splittings in $P'' = -1.5$ affect these combination differences by less than 0.0003 cm^{-1} through $J' = 7.5$. [b] This means the upper state of the line has the listed rotational parity.

strong, and have comparable intensities. Band 'C', as will be discussed later, unexpectedly has the 'f' parity-like states missing for $P' = P'' = 3/2$. The three new band systems are grouped into four identified sets in Tables 2, 4 and 5. The old band can be found in the previous work.[2]

Band A

As can be seen in Table 2, this weak band is dominated by Q- and R-branch lines with very few P-branch lines being observed. In a perpendicular band, the rotational line strengths of transitions with $\Delta J = -\Delta P$ and $P > 0$, *i.e.* P-branch lines for positive quantum number P, are smaller than those of the corresponding Q- and R-branches, but this effect seems too small to account for the absence of so many P-branches. Note that there is no parity-type splitting of the $P' = 5/2$ levels which have A_1, A_2 symmetry.

As mentioned above, a quadratic in $J'(J' + 1)$ can be fitted to the upper state energies for each sub-band. The results are shown in Table 3. It can be seen from this table that the fits are excellent except for $P' = 1/2$, and the values of the effective B rotational constants are reasonable though considerably larger than those of the ground $^2E_{3/2}$ state more closely resembling those of the $E_{1/2}$ fine structure component of the vibrationless state.

When the E_0 values are plotted against P' and fitted with a quadratic, the curvature is 4.06 cm^{-1} *vs.* 4.25 cm^{-1} for the ground state.

Band B

Since the frequencies of band 'B' were previously reported, there is no reason to repeat them here. The band is of the $P + 1 \leftarrow P$ type. The results of the same fitting procedure on Band B as that described above for Band A are given in Table 3. It is substantially stronger than Band A and has effective rotational constants that are very similar to the ground state. There is nothing unusual about finding negative effective D values for states at this energy. When E_0 is plotted *vs.* P', the curvature is almost identical with that of the ground state. There is no discernible A_1, A_2 splitting of the $P' = 5/2$ level, but the $P' = -1/2$ level does exhibit such splittings. These are plotted *vs.* J' in Fig. 5 in comparison with the A_1, A_2 splittings of the $P'' = 3/2$ level of the ground state. In this figure, the A_1, A_2 splittings for the ground state and band D have been fitted with a quadratic in $J(J + 1)$ while the curve for band B $P' = -1/2$ uses a simple interpolation procedure.

Table 2 "A" band transitions and upper state energies

J'	$E(J')$	$P\ (J'' = J' + 1)$		$Q\ (J'' = J')$		$R\ (J'' = J' - 1)$	
		ν	δ^a	ν	δ^a	ν	δ^a
$P = 0.5 \leftarrow -0.5$							
0.5	2855.5328	2843.3462	23	2846.0900	−23		
1.5	2858.7820	2842.0118	−7	2846.5938	7		
2.5	2863.6966	2840.5129	−11	2846.9252	−19	2851.5108	30
3.5	2870.5619	2839.1352	10	2847.3808	10	2853.7908	−20
4.5	2879.5005			2848.0740	17	2856.3162	−17
$P = 1.5 \leftarrow 0.5$							
1.5	2863.0680			2860.3167	−4	2863.0684	4
2.5	2868.0203			2860.6860	14	2865.2681	−14
3.5	2874.9392			2861.1846	−2	2867.6038	2
4.5	2883.8143			2861.8081	10	2870.0588	−10
5.5	2894.6284			2862.5342	0	2872.6211	0
6.5	2907.3710			2863.3560	4	2875.2764	−4
$P = 2.5 \leftarrow 1.5$; u.s. *e*							
2.5	2880.7287			2874.2463	3	2878.8352	−3
3.5	2887.7399	2866.5894	16	2874.8333	9	2881.2581	−25
4.5	2896.7240	2865.4861	1	2875.5557	7	2883.8242	−8
5.5	2907.6603			2876.3931	4	2886.5078	−4
6.5	2920.5341			2877.3300[b]	−4	2889.2961	4
$P = 2.5 \leftarrow 1.5$; u.s. *f*							
2.5	2880.7274			2874.2463	−18	2878.8352	18
3.5	2887.7406	2866.5713	−3	2874.8418	2	2881.2581	1
4.5	2896.7240	2865.4566	1	2875.5723	4	2883.8159	−5
5.5	2907.6599			2876.4226	7	2886.4902	−7
6.5	2920.5321			2877.3750[b]	−3	2889.2646	3
$P = 3.5 \leftarrow 2.5$							
3.5	2908.8452			2888.1909	3	2894.6145	−3
4.5	2918.0248			2889.1104	0	2897.3701	0
5.5	2929.1650			2890.1545	−9	2900.2515	−9
6.5	2942.2426			2891.3015	−11	2903.2344	11
7.5	2957.2128			2892.5081	14	2906.2712	14

[a] Note: $\delta = E'' + \nu - E'$, in 10^{-4} cm^{-1}. [b] Very weak not used in fitting.

Table 3 Results of fitting rotational structure (in cm^{-1}, values in parentheses are 1σ standard errors)

Band	A	B	C	D
E_0[b]				
$P' = -1.5$			**2932.282(2)**	
-0.5		**2893.8825(3)**	2919.45 (7)	2983.061(4)
0.5	2854.87 (12)	2888.2149(4)	2914.784(9)	2977.891(1)
1.5	2859.352(2)	2891.1578(6)	**2917.956(12)**	**2981.313(3)**
2.5	**2871.942(5)**	**2902.727(4)**	2930.202(8)	2993.14 (2)
3.5	2892.680(11)	2922.99 (1)		
B'				
$P' = -1.5$			**0.9591(2)**[c]	
-0.5		**0.91102 (3)**[d]	0.9384 (56)	0.9001 (3)
0.5	1.014 (25)	0.91246 (4)	0.9619 (10)	0.9083 (2)
1.5	0.9918 (2)	0.91345 (4)	**0.9710 (9)**[e]	**0.9125 (2)**[f]
2.5	**1.0059 (4)**[g]	**0.9142 (2)**[g]	0.9921 (5)	0.9359 (11)
3.5	1.0312 (6)	0.9121 (7)		
$D' \times 10^4$				
$P' = -1.5$			**0.76 (4)**	
-0.5		**−0.24 (1)**	−0.3 (9)	−2.23 (5)
0.5	8 (9)	−0.264 (6)	0.8 (2)	−1.14 (3)
1.5	1.40 (3)	−0.226 (6)	**0.5 (1)**	**−0.91 (3)**
2.5	**1.88 (7)**	**−0.49 (3)**	1.13 (7)	−0.36 (15)
3.5	2.97 (8)	−0.36 (7)		
σ				
$P' = -1.5$			**0.002**	
-0.5		**0.0004**	0.09	0.005
0.5	0.1	0.0006	0.01	0.002
1.5	0.002	0.0006	**0.01**	**0.003**
2.5	**0.003**	0.004	0.005	0.01
3.5	0.004	0.007		

[a] Boldface should correspond to A_1, A_2 pairs, but both e and f components are not always observed. [b] Extrapolated to $J' = 0$. [c] No A_1, A_2 splittings were observed. Since the ground state A_1, A_2 splittings are not resolved, we cannot tell whether or not both e and f components are present. [d] A_1, A_2 splittings do not have normal behavior, see text and Fig. 4. [e] Only e symmetry levels were observed. [f] A_1, A_2 splittings observed see text and Fig. 4. [g] The upper state A_1, A_2 splittings are too small to be determined, but both e and f components are present.

Band C

This band is in the midst of the densest region of the spectrum making it difficult to be sure that we have not just picked out a set of sub-bands that seem reasonable. The relative intensities of the Q-branch lines of the sub-bands selected strongly suggest that all these sub-bands are parallel. As expected the Q-branches are weak for the low $|P|$ sub-bands, and for those cases where the Q-branches have more than one member, the line intensities decrease with increasing J (see Fig. 2) though not as rapidly as might be expected. The rotational constants of the sub-bands of Band C (see Table 3) vary significantly with P', but are all in the range $\sim$0.94 to 1 cm^{-1}. The ground state combination differences check out quite satisfactorily for all the sub-bands, but one of the sub-bands $P = -1/2$ is fitted very poorly by a quadratic in $J'(J' + 1)$ and fitting is somewhat poor for $P = +1/2$. However, in this dense region there are many opportunities for perturbation. When the E_0's are fitted with a quadratic in P', the resulting curvature 4.14 cm^{-1} is substantially smaller than that of the ground state, but larger than that of the A band.

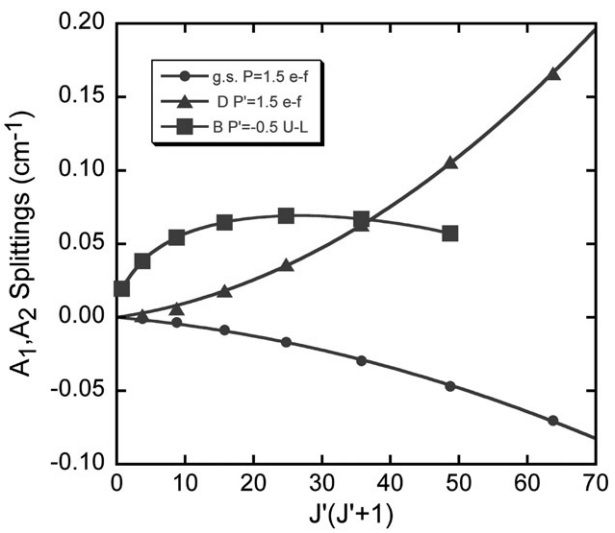

Fig. 5 A_1, A_2 splittings in ground state and B and D states.

The most disturbing aspect of Band 'C' is that only the e component of the A_1, A_2 splitting for $P' = P'' = 3/2$ is observed. We have not been able to imagine a mechanism that would lead to an A_1, A_2 splitting that does not tend to zero as J approaches zero for the simple reason that it is the end-over-end rotation that breaks Kramers degeneracy. Nor can we find a way for line strengths to depend strongly on A_1 *vs.* A_2. Therefore the most likely explanation for the missing f levels is that the $|B'_e - B'_f| \approx 0.1$ cm^{-1} giving a splitting of the

$J' = 2.5$ energy, the lowest we can test, of >0.5 cm^{-1}, and we have not been able to pick the f levels out in this crowded region.

The observed frequencies of the transitions and the average frequencies of band 'C' are given in Table 4.

Band D

The final band assigned is near the high frequency end of the spectrum, and therefore confusion in connecting its sub-bands is less of an issue, because the spectrum has become sparser. This band also obeys parallel selection rules as evidenced by rapidly decreasing Q-branch intensities as J increases. The effective B values are similar to the ground state and band B, but vary more as they increase with P'. The $P' = 2.5$ levels appear to be somewhat perturbed as evidenced by the relatively large residuals in the fit of the levels with a quadratic in $J'(J' + 1)$. The A_1, A_2 splitting in the $P' = 3/2$ level is somewhat larger than in the $P'' = 3/2$ levels of the ground state and opposite in sign (see Fig. 5). The curvature of the quadratic fit of E_0 *vs.* P' is almost exactly the same as that of the ground state.

The transition frequencies and upper state energies of band 'D', are shown in Table 5.

Fig. 6 plots the rotational constants of the four bands ABCD *versus* P'.

Additional sub-bands

We have been able to assign 10 additional sub-bands that we are unable to fit into band systems. These are listed in the ESI.§ Two of these sub-bands have $P - 1 \leftarrow P$ selection rules. The $P' = 0.5$ levels exhibit only e levels in the lower frequency sub-band with the upper sub-band having only f levels. Fig. 7 is a

Table 4 'C' band transitions and energies

J'	Upper level $E(J')$	$P(J'' = J'+1)$		$Q(J'' = J')$		$R(J'' = J' - 1)$	
		ν	δ^a	ν	δ^a	ν	δ^a
$P = -1.5 \leftarrow -1.5$							
1.5	2935.8789	2901.1218	3	2905.6948	−3		
2.5	2940.6674	2899.5061	−6	2905.9111	10	2910.4832	−4
3.5	2947.3673	2897.9741	9	2906.2061	−5	2912.6096	−4
4.5	2955.9733	2896.5164	11			2914.8115	−11
5.5	2966.4752	2895.1230	5			2917.0806	−4
6.5	2978.8569	2893.7778	−3			2919.3992	3
7.5	2993.0659[b]	2892.4307	14			2921.7119	−14
$P = -0.5 \leftarrow -0.5$							
0.5	2920.1021	2907.9131	−1	2910.6616	1		
1.5	2922.9637	2906.1934	−8			2913.5239	8
2.5	2927.7197	2904.5376	5			2915.5303	−5
3.5	2934.3347	2902.9109	44			2917.5608	−44
4.5	2942.6508	2901.1444	2			2919.4680	−2
5.5	2952.9232	2899.5061	7			2921.4944	−7
6.5	2965.3750	2898.2126	−2			2923.8687	2
7.5	2979.3908	2896.6509	1			2925.9729	−1
$P = 0.5 \leftarrow 0.5$							
0.5	2915.4953	2912.7458	14	2915.4939	−14		
1.5	2918.3968	2911.0613	1	2915.6462	2	2918.3965	−3
2.5	2923.2088	2909.4548	4			2920.4575	−4
3.5	2929.9031	2907.8918	−40			2922.5715	40
4.5	2938.5501	2906.4561	2			2924.7954	−2
5.5	2949.0736	2905.0571	−11			2927.0674	11
6.5	2961.5008	2903.7305	5			2929.4060	−5
$P = 1.5 \leftarrow 1.5$; u.s. e							
1.5	2921.6123	2915.1328	−2	2919.7185	2		
2.5	2926.4362	2913.5388	16	2919.9531		2924.5417	−13
3.5	2933.2269	2912.0745	−4			2926.7480	4
4.5	2941.9595	2910.7219	4			2929.0601	−4
5.5	2952.6128	2909.4548	−15			2931.4622	15
6.5	2965.1825	2908.2761	7			2933.9438	−7
7.5	2979.6535	2907.1641	2			2936.4968	−2
$P = 2.5 \leftarrow 2.5$							
2.5	2938.8783	2918.2234	−3	2924.6482	3		
3.5	2945.7974	2916.8831	0	2925.1428	0	2931.5671	0
4.5	2954.6839	2915.6746	2	2925.7700	5	2934.0286	−7
5.5	2965.5252	2914.5859	8	2926.5144	−12	2936.6113	4
6.5	2978.3059	2913.6011	13	2927.3660	2	2939.2949	−15
7.5	2992.9878	2912.6816	12	2928.2808	−9	2942.0474	−3

[a] $\delta = E''+\nu - E'$, in 10^{-4} cm^{-1}. [b] Omitted from fitting because of large residual.

Table 5 Band 'D'

J'	Upper level $E(J')$	$P\ (J''=J'+1)$		$Q\ (J''=J')$		$R\ (J''=J'-1)$	
		ν	δ^a	ν	δ^a	ν	δ^a
$P=-0.5\leftarrow-0.5$							
0.5	2983.7318	2971.5430	1	2974.2911	−1		
1.5	2986.4385	2969.6693	−3			2976.9977	3
2.5	2990.9581	2967.7759	3			2978.7689	−3
3.5	2997.2991	2965.8723	14			2980.5282	−14
4.5	3005.4805					2982.2968	
5.5	3015.5218	2962.1050	1			2984.0927	−1
6.5	3027.4678	2960.3047					
7.5	3041.3560	2958.6128	−32			2987.9414	32
$P=0.5\leftarrow0.5$							
0.5	2978.5719	2975.8214	4	2978.5715	−4		
1.5	2981.2988	2973.9637	6	2978.5475	−5	2981.2988	−1
2.5	2985.8462	2972.0900	−18			2983.0972	18
3.5	2992.2277	2970.2205	1			2984.8919	−1
4.5	3000.4421	2968.3485	6			2986.6871	−6
5.5	3010.5075	2966.4932	11			2988.4991	−11
6.5	3022.4443	2964.6721	−14			2990.3514	14
$P=1.5\leftarrow1.5$; *e*							
1.5	2984.7330	2978.2536	−1	2982.8391	1		
2.5	2989.3096	2976.4111	5	2982.8262	−8	2987.4167	3
3.5	2995.7184	2974.5652	−11	2982.8115	7	2989.2395	4
4.5	3003.9702	2972.7320	−2	2982.8027	15	2991.0698	−13
5.5	3014.0812	2970.9258	10	2982.8115	−22	2992.9304	12
6.5	3026.0642	2969.1570	−1			2994.8264	1
7.5	3039.9369	2967.4472	−1			2996.7805	4
$P=1.5\leftarrow1.5$; *f*							
1.5	2984.7317	2978.2484	−6	2982.8391	6		
2.5	2989.3039	2976.3957	−7	2982.8262	15	2987.4090	8
3.5	2995.7004	2974.5301	−13	2982.8027	13	2989.2178	0
4.5	3003.9344	2972.6677	9	2982.7834	10	2991.0249	−19
5.5	3014.0164	2970.8120	−25	2982.7834	33	2992.8482	−8
6.5	3025.9584	2968.9799	−12	2982.8027	8	2994.6912	4
7.5	3039.7710	2967.1814	−5			2996.5680	5
$P=2.5\leftarrow2.5$							
2.5	3001.3410	2980.6855	−8	2987.1115	8		
3.5	3007.8838	2978.9688	−6	2987.2289	−3	2993.6544	9
4.5	3016.3169	2977.3082	10			2995.6613	−9
5.5	3026.6479	2975.7079	2			2997.7333	−2
6.5	3038.8639	2974.1578	0			2999.8543	0
7.5	3052.9474	2972.6424	12			3002.0072	−12

[a] $\delta = E'' + \nu - E'$, in 10^{-4} cm^{-1}.

plot of the energies of all sub-bands relative to the energy of the lowest rotational level of the ground state *vs.* P'. The assigned bands are shown fitted with a quadratic in P'.

F. Comparison with theory

By far the most detailed calculations on the CH stretching levels are those of Marenich and Boggs[10] as shown in Fig. 4. Their final levels (rightmost in Fig. 4) are compared with our experimental results in Fig. 8. While the level spacings are similar, we can find no reasonable way to make the levels correspond when the P selection rules are taken into account. Thus in the predicted spectrum the levels reached by the red arrow should be below those reached by the blue arrows, but the reverse is true. This might be corrected by moving ν_1 up so that ν_1 $E_{3/2}$ becomes B and C and moving the ν_4 $E_{1/2}$ level connected by the blue arrow down to become Band B. If one makes this shift, there should be a black arrow band below Band B, but we have not been able to assign any full band with $P' = P'' - 1$ selection rules much less one below Band B.

Both band C and band D are rather intense. One parallel band is expected to arise from the symmetric CH stretching fundamental ν_1. It seems that the second parallel $P \leftarrow P$ band must arise from the mixing of the $E_{3/2}$ level of ν_1 with some other level. One apparent possibility is strong mixing of the $E_{3/2}$ level of ν_1 with the $E_{3/2}$ level of ν_4 through the bilinear Jahn–Teller term to create bands C and D, which are of comparable intensity.

Both this neat explanation of the origin of two strong parallel bands and the previous idea of moving ν_1 up and ν_4 down to interchange them seem implausible because of two facts: all the recent *ab initio* calculations[6,7,10] cited here find the

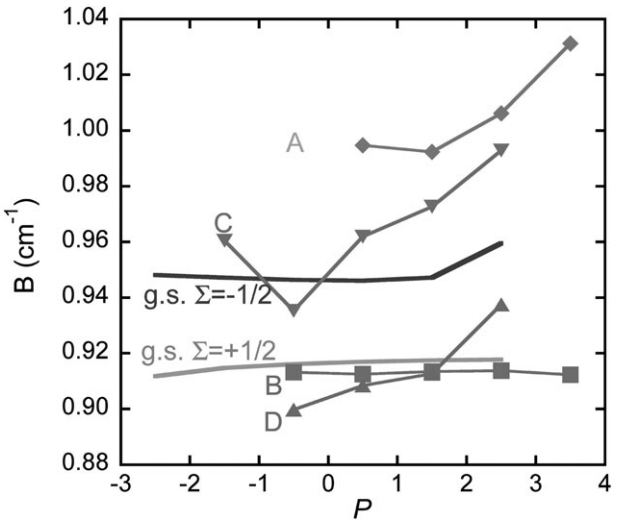

Fig. 6 Rotational constants of all assigned levels *vs.* P'.

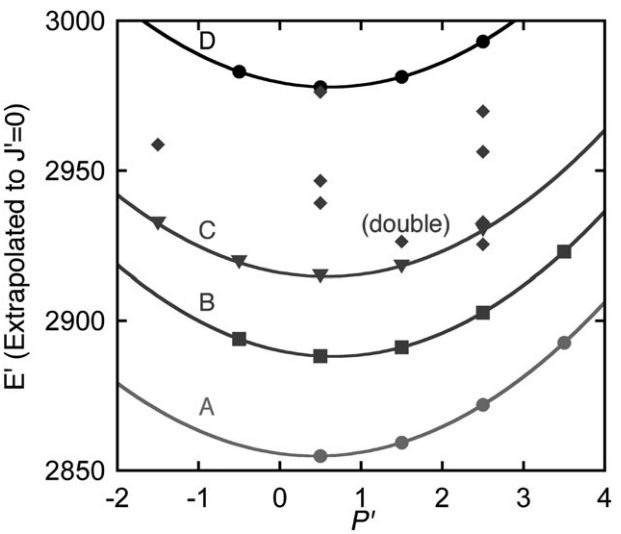

Fig. 7 Energies of all assigned sub-bands extrapolated to $J' = 0$ *vs.* P'. For some of the isolated sub-bands, P' is uncertain although P'' is known.

frequency of ν_1 lower than that of ν_4, and the analysis of the very complex spectrum of CH_3F in the CH stretching region by Giguere and Overend[14] also finds that ν_4 is higher in frequency than ν_1.

The predicted spectrum makes sense; the observed does not. We are confident that our rotational assignments of the individual sub-bands are correct and are almost as confident that the choices we have made in grouping the sub-bands into bands are correct.

Conclusion

Numerous new lines of CH_3O have been observed in the CH stretching region. Through the use of ground state combination differences, many lines have been assigned to sub-bands with definite known values of P'' with known P selection rules.

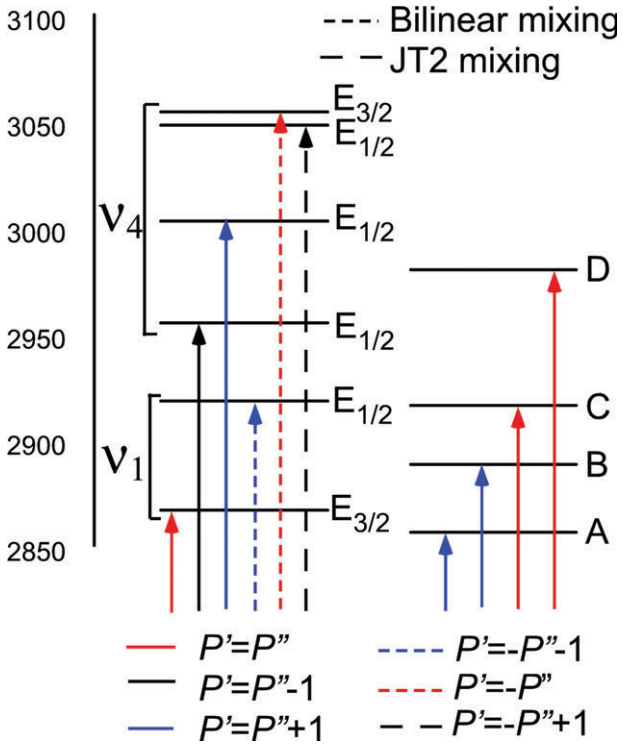

Fig. 8 Comparison of predicted (ref. 10) with observed bands in CH stretch region. (Note: We cannot distinguish the dashed and solid selection rules from the experimental spectrum.)

Three sets of these sub-bands have been grouped to form three new vibronic bands to go with the vibronic band assigned in previous work.[2] Two of these four bands have $P + 1 \leftarrow P$ selection rules and two have $P \leftarrow P$ selection rules. The richness of the spectrum in the region above 2900 cm^{-1} cannot be accounted by ν_1 and ν_4 alone as at most only 6 sub-bands, one to each of the six levels of ν_1 and ν_4, can be expected from each P'' level. There are two P' values in Fig. 7 with more than six entries. At least some of the additional sub-bands seen in Fig. 7 must be transitions to combination and/or overtone levels involving the lower frequency modes, ν_2, ν_3, ν_5, and ν_6. Unfortunately this complexity has obscured the assignment of the bands of the CH stretch fundamentals. We believe the spectrum of CH_3O in the CH stretching region may not be understood until the lower lying fundamentals and their overtones and combinations have been analyzed.

Acknowledgements

We would like to thank Referee A for suggestions and information that improved this paper significantly. Referee A brought to our attention important papers that we had failed to find and also read the paper with great care bringing to light poor wording choices and missing words.

References

1 T. A. Barckholtz and T. A. Miller, *Int. Rev. Phys. Chem.*, 1998, **17**, 435–524.

2 J. X. Han, Y. G. Utkin, H. B. Chen, L. A. Burns and R. F. Curl, *J. Chem. Phys.*, 2002, **117**, 6538–6545.
3 J. X. Han, Y. G. Utkin, H. B. Chen, N. T. Hunt and R. F. Curl, *J. Chem. Phys.*, 2002, **116**, 6505–6512.
4 L. S. Rothman, A. Barbe, D. C. Benner, L. R. Brown, C. Camy-Peyret, M. R. Carleer, K. Chance, C. Clerbaux, V. Dana, V. M. Devi, A. Fayt, J. M. Flaud, R. R. Gamache, A. Goldman, D. Jacquemart, K. W. Jucks, W. J. Lafferty, J. Y. Mandin, S. T. Massie, V. Nemtchinov, D. A. Newnham, A. Perrin, C. P. Rinsland, J. Schroeder, K. M. Smith, M. A. H. Smith, K. Tang, R. A. Toth, J. Vander Auwera, P. Varanasi and K. Yoshino, *J. Quant. Spectrosc. Radiat. Transfer*, 2003, **82**, 5–44.
5 R. Perez, J. M. Brown, Y. Utkin, J. X. Han and R. F. Curl, *J. Mol. Spectrosc.*, 2006, **236**, 151–157.
6 T. A. Barckholtz and T. A. Miller, *J. Phys. Chem. A*, 1999, **103**, 2321–2336.
7 U. Höper, P. Botschwina and H. Köppel, *J. Chem. Phys.*, 2000, **112**, 4132–4142.
8 J. Schmidt-Klugmann, H. Köppel, S. Schmatz and P. Botschwina, *Chem. Phys. Lett.*, 2003, **369**, 21–30.
9 A. V. Marenich and J. E. Boggs, *Chem. Phys. Lett.*, 2005, **404**, 351–355.
10 A. V. Marenich and J. E. Boggs, *J. Chem. Phys.*, 2005, **122**, 24308–24308.
11 A. V. Marenich and J. E. Boggs, *J. Mol. Struct.*, 2006, **780–81**, 163–170.
12 X. M. Liu, C. P. Damo, T. Y. D. Lin, S. C. Foster, P. Misra, L. Yu and T. A. Miller, *J. Phys. Chem.*, 1989, **93**, 2266–2275.
13 Y. Endo, S. Saito and E. Hirota, *J. Chem. Phys.*, 1984, **81**, 122.
14 J. Giguere and J. Overend, *Spectrochim. Acta, Part A*, 1976, **32**, 241–262.

